time. This might be a promising antimicrobial coating for a wide range of materials for biomedical or daily-life applications.

Experimental

PEI (MW 5000 g/mol) was purchased from Hyperpolymers (Freiburg, Germany). All other chemicals, if not stated otherwise, were from Fluka and used without further purification. One gram of PEI was suspended in 50 mL acetone and the mixture was cooled to 0 °C . Methacryloyl chloride (0.83 mL dissolved in 35 mL acetone) was added dropwise to the stirred suspension within 20 min. After 30 min at 0 °C, 150 mL of methanol and 20.4 mL of HEA were added to give a clear solution. The solvents were removed under reduced pressure, the PEI-MA/HEA stock solution was further diluted with HEA to control the PEI content, and 1 mg of the photoinitiator Irgacure 651 (Ciba) was dissolved in 1 mL of the solution. 20 μL of the this mixture was spread on a commercial glass slide previously modified with methacryloyloxy-propyltrimethoxysilane using a standard procedure [20]. The slide was then covered with another glass slide, previously coated with a polypropylene film. The liquid layer between the two slides was UV cured in the UV reactor Heraflash from Heraeus-Kulzer (Hanau, Germany) for 180 s to give a transparent film. The films were then washed with water/methanol/triethylamine (TEA) (1:1:1 v/v/v), water/methanol (1:1 v/v), and water, than immersed in a solution of 250 mg $AgNO_3$ in 8 mL water for 30 s, washed with water, and finally added to 50 mL of an aqueous solution of ascorbic acid (10 mg mL^{-1}). The modification of the films with PEG was performed as follows: The samples were washed with the water/methanol/TEA mixture, methanol, and acetone, then immersed into a solution of 2 g cyanuric chloride in 10 mL acetone at room temperature overnight, rinsed with acetone and chloroform, and finally left in a solution of 2 g *O*-2-aminoethyl-*O′*-methoxy polyethylene glycol (MW 5000 g/mol) in 10 mL chloroform for 24 h at room temperature. Prior to use the films were thoroughly rinsed with chloroform and immersed in a large amount of water for at least 24 h.

UV-vis measurements were carried out with the photospectrometer Lambda 11 from Perkin Elmer. AFM images were recorded with a Nanoscope III scanning probe microscope using Si cantilevers with a fundamental resonance frequency of around 200 kHz. TEM measurements were carried out using a LEO 912 transmission electron microscope applying an acceleration voltage of 120 kV. The silver content was determined using the flame-atom absorption spectrometer Vario 6 from Analytik-Jena-AG (Jena, Germany).

The bacterial susceptibility measurement was carried out according to a modified procedure described earlier [21]. *S. aureus* (ATCC 25123) cells were cultivated by adding 100 μL of a suspension of the bacterial cells in PBS (10^{11} cells/mL) to 50 mL of a standard growth medium from Merck and incubating it under shaking at 37 °C for 6 h. The bacterial suspension was then centrifuged at 2750 rpm for 10 min, the cells were washed twice with PBS, pH 7.0, re-suspended in PBS, and diluted with PBS to a concentration of 5×10^8 cells/mL controlled by the absorbance at 600 nm. The films on glass were incubated for 10 min in 50 mL of the sterile PBS and then transferred to the bacterial suspension in PBS and shaken at 200 rpm and 37 °C for 2 h with the samples standing vertically. After washing with sterile PBS three times the samples were again incubated for 1 h in PBS, washed with distilled water, and air-dried. After three minutes of drying, the samples were put into a Petri dish and 25 mL of growth agar (1.5 wt.-% agar in growth medium was heated at 100 °C for 5 min and subsequently quickly cooled to 40 °C) was added. The Petri dishes were incubated at 37 °C in an humidified incubator and the number of grown bacterial colonies was counted every 12 to 16 h.

Received: October 2, 2003
Final version: February 23, 2004
Published online: May 19, 2004

[1] J. M. Schierholz, J. Beuth, A. Rump, D.-P. Konig, G. Pulverer, *J. Chemother.* **2001**, *13*, 239.
[2] M. Edge, N. S. Allen, D. Turner, J. Robinson, K. Seal, *Prog. Org. Coat.* **2001**, *43*, 10.
[3] J. Chainer, *AISE Steel Technol.* **2001**, *78*, 59.
[4] S. D. Worley, M. Eknoian, J. Bickert, J. F. Williams, *Polymeric Drugs and Delivery Systems* (Eds: R. M. Ottenbrite, S. W. Kim), Technomic Publishing, Lancaster, PA **2000**, pp. 231–238.
[5] M. P. Pai, S. L. Pendland, L. H. Danziger, *Ann. Pharmother.* **2001**, *35*, 1255.
[6] N. P. Desai, S. F. Hossainy, J. A. Hubbell, *Biomaterials* **1992**, *13*, 417.
[7] N. Kurosaka, T. Nihei, H. Kumada, T. Umemoto, Y. Kondo, N. Yoshino, T. Teranaka, *J. Dent. Res.* **2000**, *79*, 2569.
[8] J. C. Tiller, C. J. Liao, K. Lewis, A. M. Klibanov, *Proc. Natl. Acad. Sci. USA* **2001**, *98*, 5981.
[9] Y. Ohko, Y. Utsumi, C. Niwa, T. Tatsuma, K. Kobayakawa, Y. Satoh, Y. Kubota, A. Fujishima, *J. Biomed. Mater. Res.* **2000**, *58*, 97.
[10] N. J. Szabo, J. D. Wineforder, *Anal. Chem.* **1997**, *69*, 2418.
[11] A. Blair, *Plating Surf. Finish.* **2000**, *87*, 62.
[12] D. P. Dowling, K. Donnelly, M. L. McConnell, R. Eloy, M. N. Arnaud, *Thin Solid Films* **2001**, *398–399*, 602.
[13] L. L. Woodyard, T. L. Bowersock, J. J. Turek, G. P. MyCabe, J. DeFord, *J. Controlled Release* **1996**, *40*, 23.
[14] C. Aymonier, U. Schlotterbeck, L. Antonietti, P. Zacharias, R. Thomann, J. C. Tiller, S. Mecking, *Chem. Commun.* **2002**, 3018.
[15] Z. Zhang, M. Han, *J. Mater. Chem.* **2003**, *13*, 641.
[16] H. W. Lu, S. H. Liu, X. L. Wang, X. F. Qian, J. Yin, Z. K. Zhu, *Mater. Chem. Phys.* **2003**, *81*, 104.
[17] S. Lecomte, P. Matejka, M. H. Baron, *Langmuir* **1998**, *14*, 4373.
[18] A. Abuchovski, J. R. McCoy, N. C. Palczuk, T. van Es, F. F. Davis, *J. Biol. Chem.* **1977**, *252*, 3582.
[19] Y. Xiong, M. R. Yeaman, A. S. Bayer, *Drugs Today* **2000**, *36*, 529.
[20] G. Schammler, J. Springer, *J. Adhesion Sci. Technol.* **1995**, *9*, 1307.
[21] J. C. Tiller, S. B. Lee, K. Lewis, A. M. Klibanov, *Biotechnol. Bioeng.* **2002**, *79*, 465.

Intracellular Delivery of Quantum Dots for Live Cell Labeling and Organelle Tracking**

By *Austin M. Derfus*, *Warren C. W. Chan*, and *Sangeeta N. Bhatia**

The ability to fluorescently tag and track subcellular structures in living cells represents a powerful tool in cell biology. While the time scale of observation for conventional organic

[*] Dr. S. N. Bhatia, A. M. Derfus, Dr. W. C. W. Chan[+]
Department of Bioengineering
University of California San Diego
9500 Gilman Dr. MC 0412, La Jolla, CA 92093-0412 (USA)
E-mail: sbhatia@ucsd.edu
[+] Present address: Institute of Biomaterials and Biomedical Engineering (IBBME), University of Toronto, 4 Taddle Creek Rd., Toronto, ON, M5S 3G9 Canada.

[**] We thank Dennis Young for assistance with flow cytometry, Carolan Buckmaster for microinjection, and Mike Sailor for providing facilities for QD synthesis. Funding provided by DARPA-MTO, David and Lucile Packard Foundation, NIH T32 HL07089, NIH NDDK, University of Toronto (WC), the Connaught Foundation (WC), Canadian Foundation for Innovation (WC), and Ontario Innovation Trust (WC).

DOI: 10.1002/adma.200306111

ADVANCED MATERIALS

dyes is limited due to photobleaching, semiconductor quantum dots (QDs) have surfaced as a bright, photostable alternative.[1] Furthermore, the emission properties of QDs can be tuned by size and composition, permitting the synthesis of a large set of probes to monitor many dynamic processes occurring inside living cells simultaneously. However, a key challenge in the use of QDs for intracellular tracking is the delivery of QDs to the cytoplasm and organelles such as the nucleus and mitochondria. While organic dyes used to label these organelles (DAPI, Mitotracker) are able to permeate cell membranes, the size and surface properties of QDs prevent passive diffusion across the lipid bilayer. Several groups have demonstrated the use of receptor-mediated endocytosis for intracellular delivery of QDs, but all have found that QDs entering cells by this pathway remain sequestered in endocytic vesicles, preventing the labeling of other intracellular structures.[2–4] As an alternative, one study reported the use of microinjection as a means of introducing QDs into the cytoplasm, but only to track populations of cells and not for the investigation of intracellular events.[5] Furthermore, QDs have yet to be targeted to specific organelles, proteins, or nucleic acids inside living cells to observe subcellular events. As progress is made towards the goal of real-time, multiplexed analysis of living cells, there is a need to: 1) explore alternative strategies for delivering QDs into cells, 2) develop methods to characterize and compare delivery schemes, and 3) investigate targeting strategies for labeling subcellular compartments.

With the goal of identifying an improved delivery scheme for intracellular tracking, we studied both biochemical (translocation peptides, cationic liposomes, dendrimers) and physical methods (electroporation and microinjection) of delivering QDs into cells. These approaches are commonly used for oligonucleotide delivery, however they have not been explored for delivery of semiconductor nanocrystals, despite obvious similarities in size (on the order of nanometers) and charge (negative). In order to compare these techniques qualitatively and quantitatively, we combined the use of epifluorescence microscopy to evaluate intracellular QD localization in single cells with flow cytometry to quantify the delivery efficiency over a population of live cells. To explore these methods, we coated the nanoparticles with poly(ethylene glycol) (PEG)—an inert coating that minimizes cellular uptake through endocytosis,[2] likely by preventing non-specific attachment to the cell surface, unlike other QD coatings such as silica and dihydrolipoic acid (DHLA).[3,4] Figure 1A depicts a composite (fluorescence/phase) micrograph verifying the lack of internalization of PEG-coated QDs by direct incubation with HeLa cells. Dimly fluorescent aggregates are qualitatively visible on the extracellular border. This non-specific labeling was quantified using flow cytometry, where the median cell fluorescence was measured as approximately six-fold over background (Fig. 1A, right). Furthermore, this non-specific binding was fairly uniform across a population of one million cells, as indicated by the width of the cytometry peak. In comparison, QDs that were complexed with transfection

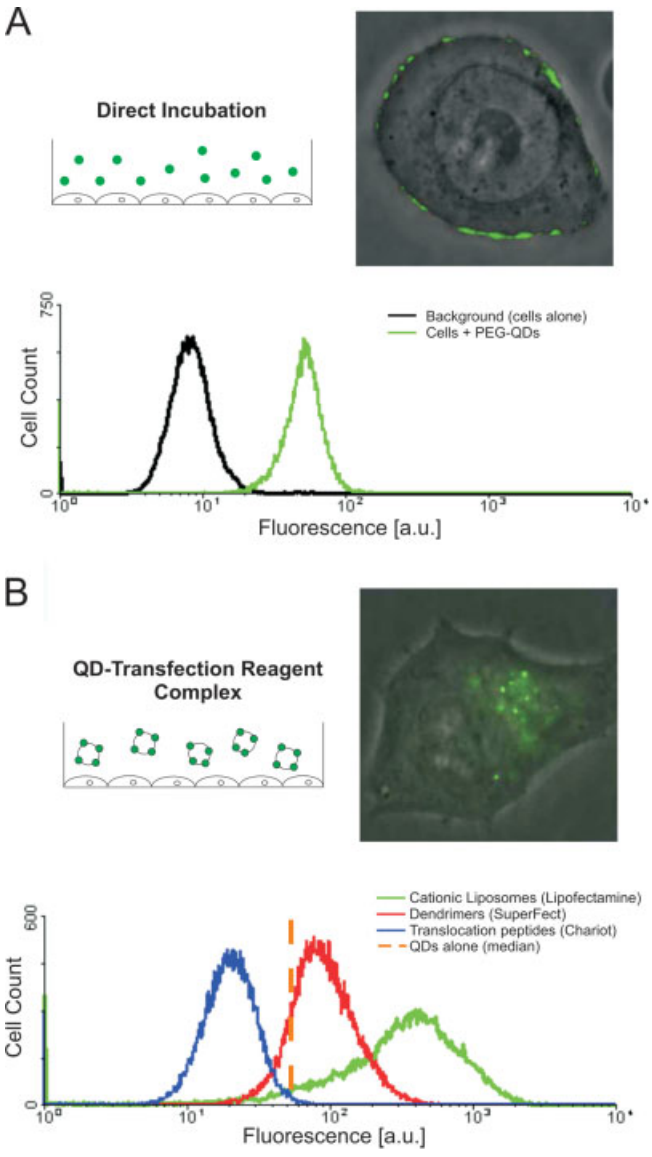

Figure 1. Improved intracellular QD delivery quantified by flow cytometry. A) Incubation of PEG-coated QDs with HeLa cells. The fluorescence/phase overlay micrograph of QDs on HeLa cells depicts dim, extracellular aggregates. Flow cytometry of cells incubated with QDs (green curve) as compared to unlabeled cells (black) demonstrates the ability to quantify labeling efficiency (graph). B) In contrast, QDs complexed with three different transfection reagents are delivered to the interior of HeLa cells (micrograph). Flow cytometry showed higher labeling efficiency of cationic liposomes (green) than dendrimers and translocation peptides (red, blue). Orange line indicates median of cells alone (from A).

reagents (translocation peptide, cationic liposome, dendrimer) prior to incubation with cells were internalized (Fig. 1B). The internalization was verified by confocal microscopy, visualizing the membrane with 5,5′-$Ph_{2D}iIC_{18}$ (Molecular Probes), a fluorescent lipophilic dye (data not shown). Flow cytometry allowed quantification of relative labeling efficiency and distribution across the cell population (Fig. 1B). Median fluorescence was highest for cationic liposomes (349 a.u.) followed by dendrimers (88 a.u.). Note that the median fluorescence

for the QD-translocation peptide complexes (20 a.u.) was unexpectedly lower than uncomplexed QDs (QDs alone, 52 a.u.), possibly due to increased scattering and quenching effects of intracellular QD aggregates compared with a disperse, extracellular fluorescence. In this case, epifluorescent microscopy provided complementary data to cytometry by indicating internalization of complexed QDs as compared to extracellular localization with uncomplexed QDs. Thus, a combination of flow cytometry and microscopy enabled the qualitative and quantitative comparison of QD delivery strategies.

In our study, cationic liposomes provided the highest delivery efficiency of QDs to live cells. Though the mechanism of delivery has not been specifically investigated in detail, we suspect that QDs behave in a similar fashion to DNA during lipofection, where DNA/liposome conjugates are formed extracellularly, endocytosed, and subsequently escape from the endosomal vesicle to access the cytoplasm.[6] Similarly, we propose that negatively charged QDs complex with cationic liposomes due to electrostatic interactions. Transmission electron microscopy was used to visualize the complexes where a single liposome measuring 200 to 500 nm in diameter was coated with approximately 20 to 40 QDs (data not shown). Subsequent cellular entry of the complexes was confirmed microscopically, and may occur through endocytosis and endosomal escape, as seen in DNA delivery. To determine whether intracellular QDs were trapped in endosomes or free in the cytoplasm, we conducted a multicolor QD experiment (Fig. 2A). Green-light-emitting QDs were complexed with the transfection agent and red-light-emitting QDs were coated by adsorption of epidermal growth factor (EGF) to promote endocytosis through the cell-surface receptor (EGFR).[7] Incubation of EGF-coated QDs yielded red-light-emitting vesicular structures that were identified as a nearly complete subset (> 95 %) of the endolysosomal compartment by co-localization with a marker for acidic organelles (LysoSensor Blue, data not shown). In contrast, QDs complexed with cationic liposomes (green) yielded a significant percentage (> 90 %) of fluorescence emission that did not co-localize with the endolysosomal compartment (red), suggesting some escape from endocytic vesicles. In principle, once QDs are free in the cytoplasm, they could be utilized to track both whole cells and intracellular processes. However, in order to fully exploit the potential of intracellular QD labeling, well-dispersed QDs are imperative. Our studies indicate that while cationic liposomes do promote efficient delivery for live cell labeling, they also form QD aggregates of several hundred nanometers in diameter that would prevent normal trafficking to the nucleus or mitochondria.[8,9]

In an attempt to deliver single, monodisperse QDs to the cell cytoplasm, we next explored the technique of electroporation. Generally used to deliver DNA to cells, electroporation temporarily generates hydrophilic pores in the plasma membrane by applying an electric field pulse. The pores allow the passive transport of DNA (or nanoparticles) into the cell.[10] Although we expected that electroporation would deliver single QDs, we instead found that aggregates of up to 500 nm in diameter were delivered (Fig. 2B, green QDs). We first suspected that the application of a high-energy electric field caused polarization of the QD surface, the loss of electrostatically-adsorbed surface ligands (PEG, mercaptoacetic acid) and subsequent QD aggregation, as has been reported for QDs in aqueous solution upon loss of stabilizing ligand.[11] To test this possibility, we delivered QDs with a crosslinked bovine serum albumin (BSA) coat[12] (which is not prone to loss of stabilizing ligand) via electroporation, and still observed clumps of QDs both inside and outside the cells. These findings suggest that stabilization of the surface ligand is not sufficient to prevent particle aggregation, and points to alternate mechanisms for aggregation. Interestingly, Golzio et al. reported that negatively charged DNA plasmids also aggregate when entering cells during electroporation.[13] They propose a model in which the electric field causes the formation of a complex between the plasmid (analogous to the nanoparticle in this case) and the cell membrane, which is internalized when membrane resealing occurs. While the mechanism of particle aggregation remains undetermined, our data suggest that electroporation under conventional conditions is a robust tool for live cell labeling with aggregated, but not monodisperse QDs. Thus, electroporation may be best utilized as a de-

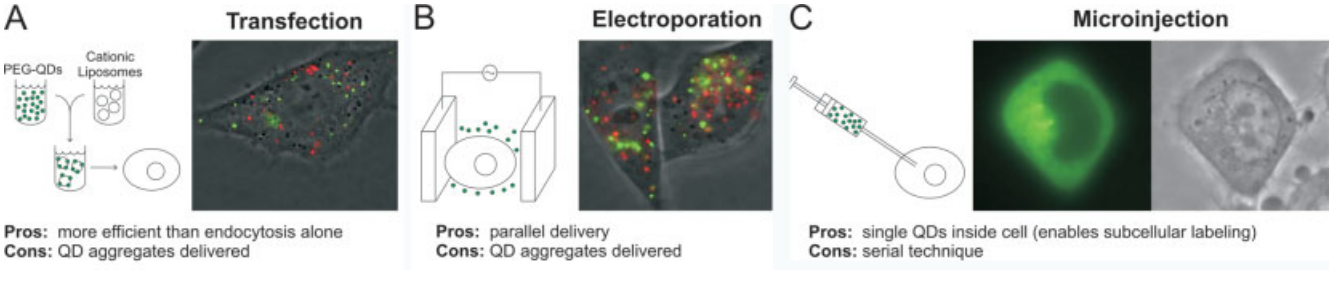

Figure 2. Comparison of delivery methods. A) Fluorescence/phase micrograph of HeLa cell transfected with green PEG-coated QDs (via complexation with cationic liposomes) and red EGF-QDs (as an endosomal label). B) Fluorescent/phase micrograph of a HeLa cell after electroporation in a solution of green QDs followed by incubation with red EGF-QDs as endosomal label. A,B) depict aggregated QDs and significant lack of green/red co-localization consistent with endosomal escape. C) Fluorescence (left) and phase (right) micrograph of HeLa cell 2 h after cytoplasmic injection of green QDs. Diffuse cytoplasmic staining is consistent with non-aggregated QDs and nuclear exclusion (though fluorescence can be seen in focal planes above and below the nucleus).

ADVANCED MATERIALS

livery scheme in applications such as whole cell tracking and cytometry.

Using these two approaches (complexing with cationic liposomes and electroporation), we have demonstrated the ability to label a large population of cells in parallel. Both techniques, however, deliver QD aggregates that are not ideal for intracellular assays. For single-cell labeling, microinjection is a superior approach, albeit a serial one, that enables delivery of QDs to the cell's interior in a monodisperse form. Figure 2C depicts the microinjection of PEG-QDs into the cytoplasm of a single cell, resulting in a diffuse cytoplasmic stain. Passive transport through the nuclear envelope is limited to substances 9 nm or less in diameter,[14] explaining the observed nuclear exclusion of the PEG-QDs (~28 nm diameter determined by dynamic light scattering (DLS)).

In order to explore the utility of monodisperse QDs for studying subcellular phenomena, we next synthesized 'multifunctional' QDs that combined narrow fluorescence emission with an inert coating (PEG) and a peptide localization sequence for delivery via microinjection. Our goal was to direct subcellular localization of the QDs by alteration of the peptide sequence, thereby enabling visualization of specific intracellular organelles. We specifically explored the use of a 23mer nuclear localization sequence (NLS) peptide and a 28mer mitochondrial localization sequence (MLS) peptide to traffic QDs to the nucleus and mitochondria respectively. The NLS peptide contains the canonical 7mer (PKKKRKV) functional domain from the SV40 T antigen plus additional residues that have been shown to increase nuclear accumulation.[15] This peptide recognizes the nuclear transport protein importin (karyopherin) alpha, leading to active transport through the nuclear pore complex.[8] Gold colloids as large as ~39 nm in diameter have been transported into the nucleus in this manner,[16] and the ~25 nm diameter PEG-QD–NLS conjugate (measured by DLS) is well below this threshold. The MLS consists of the targeting presequence from human cytochrome oxidase subunit VIII (COX8), a protein that is synthesized in the cytoplasm and actively transported into the mitochondria.[9,17] Each of these peptides was synthesized to contain a free cysteine residue, whose sulfhydryl group allowed electrostatic adsorption to the QD surface.[18] Figure 3A depicts the successful nuclear localization of the NLS-conjugated QDs as compared to the cytoplasmic distribution of the rhodamine-dextran (70 kDa molecular weight) control 18 h after microinjection. Comparison of nuclear localization of NLS-conjugated PEG-QDs to cytoplasmic localization of PEG-QDs alone (Fig. 2C) supports the conclusion that adsorption of the NLS peptide is sufficient to specify nuclear trafficking. Similarly, MLS-conjugated QDs were observed around mitochondria by 18 h, as indicated by co-localization of QDs with an organic mitochondrial dye that readily permeates the cell membrane and accumulates due to a thiol-reactive chloromethyl moiety (MitoTracker Red) in Figure 3B.[19] For both peptides, significant localization of QDs had occurred after 30 min, and additional accumulation occurred over 2 h and 18 h. No further changes were observed through 24 h. While these localization kinetics are slower than previous reports of DNA delivery to the nucleus (5–30 min),[15] they are consistent with the time scale of cytoplasmic transport of larger complexes such as intact adeno-associated viruses (~90 nm),[14] reflecting that size plays a role in localization kinetics. For these viruses, perinuclear accumulation begins within 30 min, and significant intranuclear accumulation of the smaller inner core occurs by 2 h. Possible reasons for the prolonged localization of QD bioconjugates relative to biomolecules include their relative size, as well as suboptimal live cell microscopy conditions (repeated exposure to room temperature and basic pH due to CO_2 buffering), and an excess of free localization peptide competing with QD conjugates for a fixed number of transporters. In the current report, our goal was to demonstrate proof-of-principle for use of signaling peptides to traffic quantum dot nanoparticles although the subcellular localization kinetics of nanoparticle bioconjugates merit further study.

Finally, in order to demonstrate the feasibility of tracking organelles without photobleaching limitations, we monitored labeled mitochondria in live cells over eight minutes of continuous exposure with no measurable loss in signal intensity (Fig. 3C). In comparison, dye-labeled mitochondria photobleached beyond detection in less than 30 s (Fig. 3D). Collectively, these experiments demonstrate that the use of peptide localization sequences and PEG coating in conjunction with microinjection enable the delivery and subcellular localization of QDs in live cells. The appropriate intracellular trafficking of conjugated QDs is consistent with the persistence of both PEG (required to prevent aggregation) and localization peptides (required for targeting) on the QD surface even in the intracellular biochemical milieu, thereby suggesting that adsorption of a thiolated peptide is an adequate method of QD conjugation for at least some intracellular assays.

In conclusion, we have explored and characterized several strategies to enhance delivery of QDs to live cells using epifluorescent microscopy and flow cytometry. Endocytosis of QDs results in sequestration of the majority of QDs in the endolysosomal compartment where they are unavailable for subsequent intracellular assays. Delivery of QD/cationic liposome complexes and electroporation are efficient schemes to deliver QDs to the cytoplasm of a large population of cells, yet QDs form large aggregates that can restrict subsequent trafficking (e.g., passage through nuclear pores). In contrast, microinjection delivers QDs to the cell interior as monodisperse nanoparticles, but requires each cell to be individually manipulated. Using microinjection of QD-PEG peptide conjugates, we demonstrated the ability to target QDs to subcellular sites using known localization sequences. In fact, a plethora of localization sequences exist to extend our findings to the labeling of other organelles (endoplasmic reticulum, golgi, peroxisomes, etc.). Moving forward, the ability to deliver and target QDs to intracellular sites will help to realize the promise of these versatile nanoparticles.

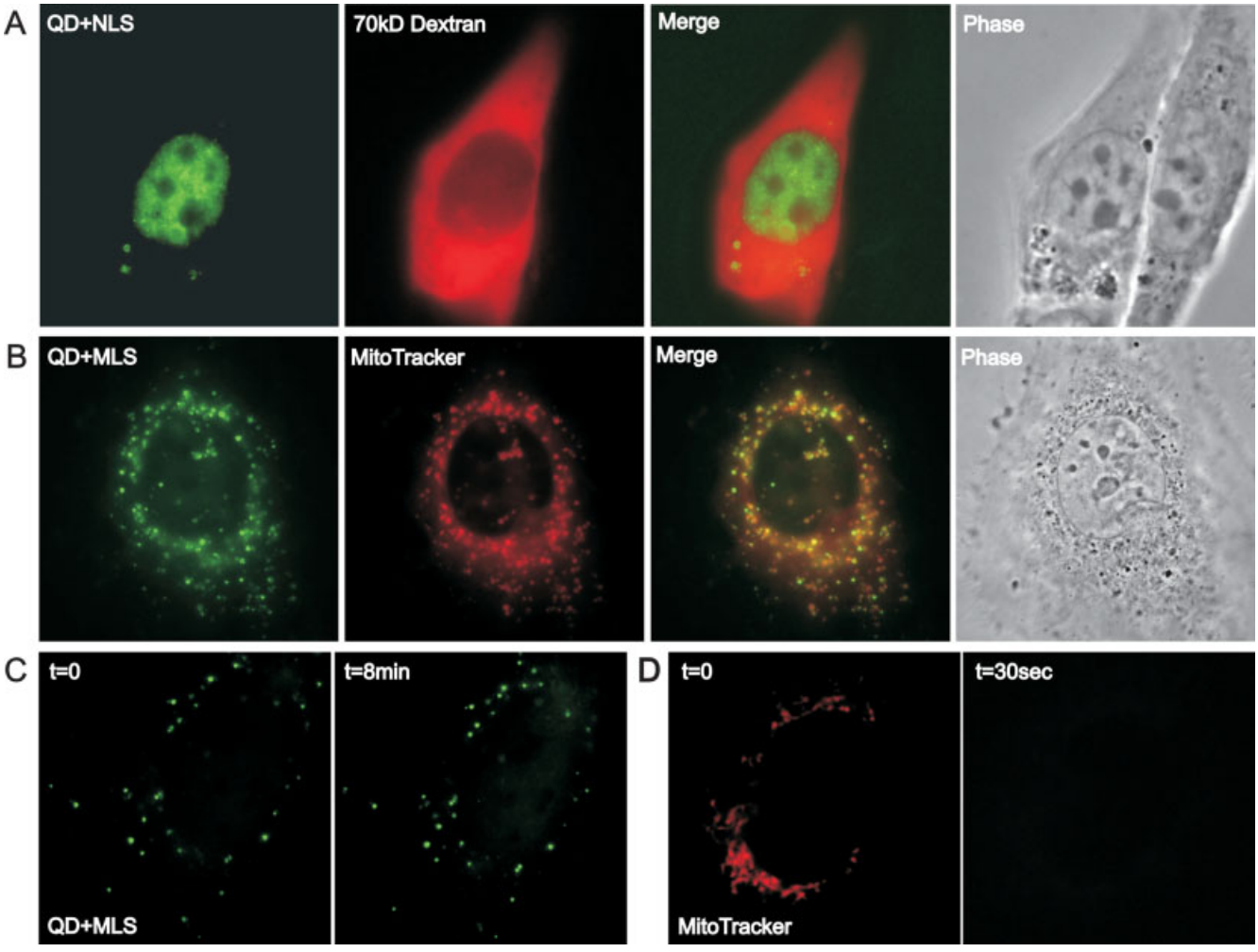

Figure 3. Subcellular localization of single QDs. PEG-QDs were conjugated to localization sequence peptides, which permit active transport to the nucleus. (NLS, A) or mitochondria (MLS, B), and were delivered to 3T3 fibroblast cells by microinjection. A) Fluorescence and phase micrographs of a HeLa cell 24 h after co-injection of NLS-QDs with 70 kDa rhodamine dextran control. The four spots in the nucleus that are not stained with QDs are the nucleoli, and are also seen on the phase image. B) Fluorescence and phase micrographs 24 h after injection of MLS-QDs. Co-localization with Mitotracker Red confirms mitochondrial labeling. C) QDs remain fluorescent after 8 m of continuous mercury lamp exposure, while conventional MitoTracker dye (D) bleaches beyond detection after 30 s of continuous excitation. Different cells were imaged for (C,D).

Experimental

Quantum Dot Preparation: CdSe/ZnS nanocrystals were synthesized [20,21] and water-solubilized with mercaptoacetic acid (MAA) as previously described [2]. For PEG-QDs, methoxy poly(ethylene glycol) amine (mPEG–NH_2, 5000 MW) (Shearwater) was reacted with equimolar 2-iminothiolane (Sigma) to add a thiol group, and then conjugated directly to MAA-QDs via a thiol exchange reaction [22]. For EGF-QDs, epidermal growth factor (EGF, Becton Dickinson Biosciences) was thiolated with equimolar 2-iminothiolane and reacted with PEG-QDs at room temperature for several hours. Green (550 nm emission maxima, 40 nm full width at half maximum (FWHM)) and red QDs (630 nm emission maxima, 38 nm FWHM) were used for these experiments.

Transfection-Agent-Assisted QD Labeling: Transfection reagents from three different classes were used—cationic liposomes (Lipofectamine 2000, Invitrogen), activated dendrimers (Superfect, Qiagen), and translocation peptides (Chariot, Active Motif). The reagents were applied to cells based on the manufacturer's instructions for DNA/protein transfection. Briefly, 10 μL of transfection reagent in Dulbecco's Modified Eagles' Medium (DMEM) and 15 μg of QDs in DMEM were used for each 35 mm well (80 % confluent) and allowed to complex. For Chariot, the protocol was altered slightly (6 μL reagent in water complexed with QDs in phosphate-buffered saline (PBS)). The QD/reagent solutions were diluted in DMEM (to 1 mL per well) and incubated with the cells. Six hours later, the transfection media was removed and DMEM with 10 % FBS (fetal bovine serum) and pen/strep (penicillin/streptomycin) was added. Approximately 6 h later, the cells were trypsinized and prepared for flow cytometry or re-plated on glass coverslips for imaging. All cell images were captured by a cooled CCD (charge-coupled device) camera (CoolSnap HQ, Roper Scientific) and processed on MetaVue software (Universal Imaging). Flow cytometry was performed on a FACSCalibur (BD Biosciences) with a 488 nm Ar laser. Signal from the FL1 bandpass emission (530/30) was used for the green QDs and WinMDI software (http://facs.scripps.edu) was used to generate population histograms.

ADVANCED MATERIALS

Electroporation: A BTX 600 electro cell manipulator was used to deliver PEG-QDs to HeLa cells. Electroporation parameters were varied using several solutions (phosphate-buffered saline, Krebs Ringers Buffer, Dulbecco's Modified Eagles' Medium, and HEPES-buffered (HEPES—4-(2-hydroxyethyl)piperazine-1-ethanesulfonic acid) isotonic glucose solution), charging voltages (100–500 V), and pulse lengths (0.5–20 ms). Optimal intracellular delivery without extensive cell death (greater than 50 % viability) occurred in PBS with a single 100–200 V, 1–5 ms pulse. Approximately 10^6 cells were suspended in 400 μL of DMEM with 250 $\mu g\,mL^{-1}$ QDs. The electroporation charge was applied, and, after 10 min, the cells were pelleted to remove the QD solution, and then plated on coverslips. All steps were performed at 4 °C to prevent endocytosis of QDs.

Received: September 3, 2003
Final version: February 5, 2004
Published online: May 19, 2004

[1] W. C. Chan, D. J. Maxwell, X. Gao, R. E. Bailey, M. Han, S. Nie, *Curr. Opin. Biotechnol.* **2002**, *13*, 40.
[2] W. C. Chan, S. Nie, *Science* **1998**, *281*, 2016.
[3] W. J. Parak, R. Boudreau, M. Le Gros, D. Gerion, D. Zanchet, C. M. Micheel, S. C. Williams, A. P. Alivisatos, C. Larabell, *Adv. Mater.* **2002**, *14*, 882.
[4] J. K. Jaiswal, H. Mattoussi, J. M. Mauro, S. M. Simon, *Nat. Biotechnol.* **2003**, *21*, 47.
[5] B. Dubertret, P. Skourides, D. J. Norris, V. Noireaux, A. H. Brivanlou, A. Libchaber, *Science* **2002**, *298*, 1759.
[6] I. S. Zuhorn, D. Hoekstra, *J. Membr. Biol.* **2002**, *189*, 167.
[7] R. Brock, T. M. Jovin, *J. Cell Sci.* **2001**, *114*, 2437.
[8] L. F. Pemberton, G. Blobel, J. S. Rosenblum, *Curr. Opin. Cell Biol.* **1998**, *10*, 392.
[9] R. Rizzuto, H. Nakase, B. Darras, U. Francke, G. M. Fabrizi, T. Mengel, F. Walsh, B. Kadenbach, S. DiMauro, E. A. Schon, *J. Biol. Chem.* **1989**, *264*, 10 595.
[10] T. Y. Tsong, *Biophys. J.* **1991**, *60*, 297.
[11] X. Gao, W. C. Chan, S. Nie, *J. Biomed. Opt.* **2002**, *7*, 532.
[12] A. M. Derfus, W. C. Chan, S. N. Bhatia, *Nano Lett.* **2004**, *4*, 11.
[13] M. Golzio, J. Teissie, M. P. Rols, *Proc. Natl. Acad. Sci. USA* **2002**, *99*, 1292.
[14] K. H. Bremner, L. W. Seymour, C. W. Pouton, *Curr. Opin. Mol. Ther.* **2001**, *3*, 170.
[15] S. Hubner, C. Y. Xiao, D. A. Jans, *J. Biol. Chem.* **1997**, *272*, 17 191.
[16] N. Pante, M. Kann, *Mol. Biol. Cell* **2002**, *13*, 425.
[17] G. Manfredi, J. Fu, J. Ojaimi, J. E. Sadlock, J. Q. Kwong, J. Guy, E. A. Schon, *Nat. Genet.* **2002**, *30*, 394.
[18] The NLS peptide, NH_2–CSSDDEATADSQHSTPPKKKRKV–COOH, and MLS peptide, NH_2–MSVLTPLLLRGLTGSARRLPV-PRAKIHC–$CONH_2$, were commercially synthesized (Global Peptide).
[19] M. Poot, Y. Z. Zhang, J. A. Kramer, K. S. Wells, L. J. Jones, D. K. Hanzel, A. G. Lugade, V. L. Singer, R. P. Haugland, *J. Histochem. Cytochem.* **1996**, *44*, 1363.
[20] C. B. Murray, D. J. Norris, M. G. Bawendi, *J. Am. Chem. Soc.* **1993**, *115*, 8706.
[21] M. A. Hines, P. Guyot-Sionnest, *J. Phys. Chem.* **1996**, *100*, 468.
[22] M. E. Akerman, W. C. Chan, P. Laakkonen, S. N. Bhatia, E. Ruoslahti, *Proc. Natl. Acad. Sci. USA* **2002**, *99*, 12 617.

Free-Standing Gold Nanoparticle Membrane by the Spontaneous Reduction of Aqueous Chloroaurate Ions by Oxyethylene-Linkage-Bearing Diamine at a Liquid–Liquid Interface**

By *PR. Selvakannan*, *P. Senthil Kumar*, *Arvind S. More*, *Rahul D. Shingte*, *Prakash P. Wadgaonkar*, and *Murali Sastry**

The combination of nanoscale inorganic materials with organic polymers has immense potential for future applications such as device technology, separation methodologies, and drug delivery and consequently has attracted considerable attention during the last decade.[1–3] Polymeric systems have played important roles as templates with different morphologies and tunable sizes for nanofabrication of a range of inorganic materials, as they can be easily removed after reaction and can be further modified with different functional groups to enhance interaction with the guest.[2]

Incorporating nanoparticles into the polymer matrices using external porous membranous templates is a well-known procedure.[4–7] There is increasing interest in using such synthetic membranes, particularly in biological applications such as protein separation and tissue engineering.[4–7] Potential advantages of membrane-based protein separations include low cost, high speed, and high throughput of the process. In addition, membrane-based separations can, in principle, be scaled up for large-scale use in commercial production. Gold nanotubule membranes are ideal model systems to explore how pore size affects the rate and selectivity of protein transport in synthetic membranes.[4–7]

Development of experimental methods for the in situ generation of nanoparticles in a polymeric matrix during the polymerization process itself opens up much wider possibilities for macromolecular applications.[1] There are very few reports on the synthesis of inorganic-nanoparticle–polymer composite structures wherein the metal ions and monomers in solution react spontaneously to yield such composites.[8] Tamil Selvan and co-workers have shown that the reduction of $AuCl_4^-$ ions sequestered in micelles of a diblock copolymer

[*] Dr. M. Sastry, PR. Selvakannan, Dr. P. S. Kumar
Materials Chemistry Division
National Chemical Laboratory
Pune-411008 (India)
E-mail: sastry@ems.ncl.res.in
A. S. More, R. D. Shingte, Dr. P. P. Wadgaonkar
Polymer Chemistry Division
National Chemical Laboratory
Pune-411008 (India)

[**] PR. S, P. S. K., and R. D. S. thank the Council of Scientific and Industrial Research (CSIR), Govt. of India for research fellowships. Ms. Renu Pasricha and Dr. A. B. Mandale are acknowledged for assistance with TEM and XPS measurements respectively.

  DOI: 10.1002/adma.200400116